

Measurement report: Analysis of aerosol optical depth variation at Zhongshan Station in Antarctica

Lijing Chen^{1,2}, Lei Zhang¹, Yong She², Zhaoliang Zeng¹, Yu Zheng¹, Biao Tian¹, Wenqian Zhang¹, Zhaohui Liu³, [Huizheng Che¹](#), Minghu Ding^{*1}

¹ State Key Laboratory of Severe Weather, Chinese Academy of Meteorological Sciences, Beijing, 100081, China.

² Chengdu University of Information Technology, Chengdu, 610103, China.

³ Polar Surveying and Mapping Engineering Center of Heilongjiang Administration of Surveying, Mapping and Geoinformation, Harbin 150081, China

Correspondence to: Minghu Ding (dingminghu@foxmail.com)

Three key findings:

- The AOD level over Zhongshan Station in Antarctica is low in summer and high in winter. AE indicates the dominance of fine (coarse) aerosols in summer (winter).

- ~~In winter and spring, high AOD values are related to the increase of coarse mode particles, while in summer and autumn, high AOD values may be related to the growth of fine mode particles. The increase in AOD during spring and winter correlates with a reduction in the fine mode fraction, whereas the increase observed in summer and autumn may be attributed to the growth and aging of fine particles.~~

- AOD varied inversely with wind speed and showed an insignificant positive correlation with temperature but a significant negative correlation with relative humidity.

Abstract: Our understanding of aerosol optical depth (AOD) in Antarctica remains limited due to the scarcity of ground observation stations and limited daylight days. Utilizing data from the CE318-T photometer spanning from January 2020 to April 2023 at Zhongshan Station, we analysed the seasonal, monthly, and diurnal variations in AOD and Ångström exponent (AE). AOD median values increased from spring (0.033) to winter (0.115), while AE peaked during summer (1.010) and autumn (1.034), declining in winter (0.381), indicating a transition in dominant aerosol particle size from fine to coarse mode between summer and winter. Monthly mean AOD variation closely paralleled the proportion of $AE < 1$, suggesting fluctuations in coarse mode particle proportions drive AOD variation. [The high AOD](#)

30 values during winter and spring were associated with increased contribution of coarse mode particles,
31 while high AOD values during summer and autumn were associated with the growth of fine mode
32 particles. Increases in AOD during spring and winter correlated with decreases in fine mode fraction,
33 while increases during summer and winter related to fine mode particle growth and aging. We observed
34 a peak in AOD (~0.06) at 14:00 local time at Zhongshan Station, possibly associated with a slight
35 decrease in boundary layer height (BLH). Additionally, higher (lower) wind speeds corresponded to
36 lower (higher) AOD values, indicating the diffusion (accumulation) effect. The temperature and AOD
37 showed an insignificant positive correlation ~~between~~ ($R = 0.22$, $p = 0.40$), relative humidity exhibited a
38 significant negative correlation with AOD ($R = -0.59$, $p = 0.02$). Backward trajectory analysis revealed
39 that coarse particles from the ocean predominantly contributed to high AOD daily mean values, while
40 fine particles on low AOD days originated mainly from the air mass over the Antarctic Plateau. ~~Backward~~
41 ~~trajectory analysis revealed that coarse particles from the ocean predominantly contributed to high AOD~~
42 ~~daily mean values in summer, while fine particles on low AOD days originated mainly from the air mass~~
43 ~~over the Antarctic Plateau.~~
44 This study enhances the understanding of the optical properties and seasonal behaviors of aerosols in the
45 coastal Antarctic. Specifically, AOD measurements during the polar night address the lack of validation
46 data for winter AOD simulations. Additionally, we revealed that lower wind speeds, higher temperatures,
47 and lower relative humidity contribute to increased AOD at Zhongshan Station, and air masses from the
48 ocean significantly impact local AOD levels. These findings help us infer AOD variation patterns in the
49 coastal Antarctic based on meteorological changes, providing valuable insights for climate modeling in
50 the context of global climate change.

51 **1 Introduction**

52 Aerosols play an important role in impacting the climate system by absorbing and scattering solar
53 radiation (Li et al., 2022). Antarctica, considered one of the most pristine lands, serves as an ideal
54 background area for evaluating the climate effects of aerosols (Kamra, 2022). Marine aerosols emitted
55 from the Southern Ocean are a primary source contributing to the aerosol load in ~~the~~ Antarctica (Thakur,
56 2019). The retreat of sea ice in Antarctica is expected to escalate the release of sea salt and secondary

57 biogenic aerosols (Yan et al., 2020). Sea salt particles with strong scattering may produce negative
58 effective radiative forcing or indirect radiative effect by influencing cloud condensation nuclei within
59 the marine boundary layer over Antarctica (Thornhill et al., 2021; Udisti et al., 2012). However, the
60 heating effect of absorbent aerosols, such as black carbon (BC), may be amplified by the high surface
61 albedo in Antarctica (Kang et al., 2020). In recent years, there has been a notable increase in BC
62 concentrations in Antarctica, with BC deposition on snow and ice surfaces contributing to reduced
63 surface albedo and increased solar radiation absorption, subsequently accelerating snow and ice melt
64 (Kannemadugu et al., 2023). Given the close connection between aerosol radiation effects and their
65 optical properties (Che et al., 2024), it is necessary to investigate the optical parameters of Antarctica
66 aerosols.

67 Aerosol optical depth (AOD), as a key parameters of aerosol optical properties, serves as an effective
68 measure of aerosol load and can influence the solar radiation components (Alghoul et al., 2009). AOD
69 observation records from Antarctica sites indicate that the ~~mean-values~~ range from ~~0.02-006~~ to ~~0.220~~ in
70 coastal regions and from ~~0.005-007~~ to ~~0.034~~ in inland regions (Kannemadugu et al., 2023; Tomasi et al.,
71 2007, 2012; Yang et al., 2021). Typically, coastal aerosols consist primarily of coarse-mode sea salt
72 particles during austral winter, while fine-mode particles (such as dimethyl sulfide and its oxidation
73 product mesylate, DMS, and MSA) lead to elevated particle number concentrations in summer (20-100
74 times higher than in winter) (Lachlan-Cope et al., 2020; Shaw, 1979). Conversely, aerosols over the
75 Antarctic Plateau predominantly comprise fine-mode particles of non-sea-salt sulfate (NSS) and DMS
76 (Harder et al., 2000; Walters et al., 2019).

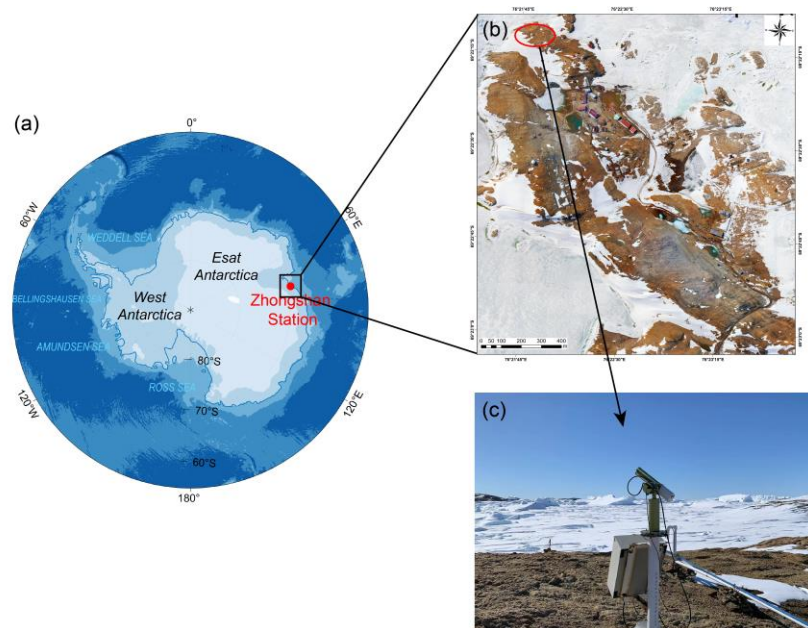
77 Additionally, particle size plays a significant role in aerosol extinction. The Ångström exponent (AE)
78 serves as an important indicator of aerosol size, with value greater (less) than 1 indicating a predominance
79 of fine (coarse) mode particles (Schuster et al., 2006). Weller and Lampert report that the mean AE at
80 Neumayer Station was 1.5 ± 0.6 and 1.2 ± 0.5 during summer and winter, respectively, suggesting an
81 increased contribution of fine-mode biological sulfate particles in summer (Weller and Lampert, 2008).
82 Virkkula et al. observed higher scattering AE estimate values during summer (~ 1.9) and lower values
83 during winter (~ 0.8) at Dome C on the Antarctic Plateau, indicating a prevalence of fine particles in
84 summer (Virkkula et al., 2022).

85 Currently, the challenging environment and the limited number of daylight days per year restrict the
86 availability of ground sites capable of obtaining adequate AOD and AE observations. Consequently, the
87 optical properties of aerosols across large parts of Antarctica remain unexplored. To improve our
88 comprehension of aerosol properties in Antarctica, we analyse the seasonal, monthly, and diurnal
89 variations of AOD and AE using data obtained from the recently installed sun-sky-lunar CE318-T
90 photometer at Zhongshan Station.

91 **2 Site, Instrument, and Data**

92 **2.1 Site Introduction**

93 Zhongshan Station (69°22'12"S, 76°21'49"E, 18 m a.s.l.) is located at the Larsemann Hills of Prydz Bay
94 on the east Antarctic continent. The sun-sky-lunar CE318-T photometer is installed at Swan Ridge,
95 northwest of the Nella fjord (Fig. 1) (Tian et al., 2022). This location experiences 54 polar days and 58
96 polar nights annually, with snow covering the surrounding surface during winter and revealing bare rock
97 in summer. In this study, the austral spring, summer, autumn, and winter are referred to the season from
98 September to November (SON), December to February of next year (DJF), March to May (MAM), and
99 June to August (JJA), respectively. The average annual air temperature is $-10\text{ }^{\circ}\text{C}$, with a relative
100 humidity of 58% and prevailing wind speeds of 6.9 m s^{-1} , primarily from the east or east-southeast
101 direction (Ding et al., 2022).



102
 103 **Figure 1 (a) The location of Zhongshan Station in Antarctica, (b) the aerial view of Zhongshan Station, and**
 104 **(c) the sun-sky-lunar photometer CE318-T at Zhongshan Station.**

105 **2.2 Instrument and Data**

106 The AOD measurement data utilized in this study were obtained from the sun-sky-lunar CE318-T
 107 photometer, manufactured by CIMEL Electronique, France. The CE318-T is a ground-based multiband
 108 radiometer capable of inverting aerosol optical parameters by measuring the spectral data of direct solar
 109 and lunar radiation extinction and the angular distribution of sky radiances (Barreto et al., 2016).

110 We collected AOD level 1.5 (cloud-screened) data across various wavelengths spanning from January
 111 2020 to April 2023 (Fig. S1). However, the operation of CE318-T in polar environment is impeded by
 112 solar radiation and weather conditions, leading to a significant number of missing measurements.

113 Consequently, we categorize daily observations with less than 20 measurements and the coefficient of
 114 dispersion (CV) exceeding 1 as invalid data, which are systematically eliminated from our analysis.

115 Typically, these invalid data manifest with exceedingly high AOD values, often attributed to instrument
 116 downtime caused by factors such as precipitation or cloudy weather. Moreover, to ensure the accuracy
 117 of AOD measurement at Zhongshan Station, we refine our data by cross-referencing station operation
 118 records and the time series of black carbon (BC) concentrations. This process allows us to exclude AOD
 119 data associated with significant station activities and periods of elevated BC concentrations, thereby
 120 enhancing the reliability of our analysis. It should be noted that there are uncertainties in the AOD

121 measurements of CE318-T during field observations due to atmospheric conditions, instrument noise,
122 and calibration. It is estimated that during daytime measurements, the AOD uncertainty ranges from
123 0.010 to 0.021. For night-time measurements, the AOD uncertainty depends on the calibration technique
124 used. Specifically, when calibrated using the Moon Ratio technique, the uncertainty ranges from 0.011
125 to 0.019. With the application of the new Sun Ratio technique, the uncertainty for the 440 nm channel is
126 between 0.012 and 0.015 (0.017), while for longer wavelengths, it ranges from 0.015 to 0.021. By
127 employing the new Sun-Moon gain factor technique and using the Langley-calibrated instrument for
128 calculation of the amplification between daytime and night-time measurements, the uncertainty range is
129 from 0.016 to 0.019 (Barreto et al., 2016).

130 The meteorology data, including temperature, relative humidity, wind direction, and wind speed, were
131 obtained from the Zhongshan Station meteorology observatory, with the temporal resolution of 1 hour.
132 BLH data was obtained from ERA5 reanalysis provided by European Centre for Medium Range Weather
133 Forecasts (ECMWF) with the temporal and spatial resolution of 1 hour and 0.25 (latitude) × 0.25
134 (longitude).

135 The Hybrid Single-Particle Lagrangian Integrated Trajectory (HYSPPLIT) model, is a comprehensive
136 model developed by the National Oceanic and Atmospheric Administration (NOAA) and the Air
137 Resources Laboratory (ARL) to calculate and analyse the source, transport, and diffusion trajectories of
138 atmospheric pollutants. The meteorological data used in the HYSPLIT model comes from the National
139 Center for Environmental Prediction (NCEP) Global Data Assimilation System (GDAS). In this study,
140 the HYSPLIT model is utilized to calculate the 168h backward air mass trajectory from 3 altitudes of
141 50,500 and 1000 m (amsl) to Zhongshan Station.-

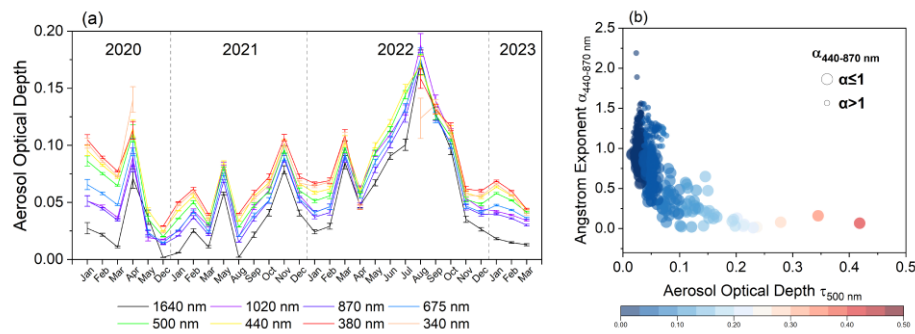
142 **3 Results**

143 **3.1 Variation Characteristics of AOD**

144 From January 2020 to March 2023, the monthly mean AOD values at various wavelengths varied from
145 0.00 to 0.20, with the lowest values in December 2020 and the highest values in August 2022 (Fig. 2a).

146 The monthly mean AOD values at 500 nm (AOD_{500 nm}) generally remained below 0.10, consistent with
147 findings by Gadhavi and Achuthan at the Maitri Station, where AOD variation fell within the range of

148 0.01 to 0.10 (Gadhavi and Achuthan, 2004). The annual mean \pm SD (standard deviation) values of the
 149 AOD_{500 nm} were 0.074 \pm 0.090, 0.051 \pm 0.066, 0.071 \pm 0.117, and 0.053 \pm 0.031 in 2020, 2021, 2022, and
 150 2023, respectively (Table 1). Similarly, the annual mean \pm SD values of the AE_{440-870 nm} were
 151 1.134 \pm 0.411, 0.953 \pm 0.338, 0.883 \pm 0.374, 0.753 \pm 0.206 in 2020, 2021, 2022, and 2023 for the same
 152 years, respectively, which suggests suggesting that the aerosols over Zhongshan Station were mainly
 153 dominated by fine mode particles in 2020, and coarse mode particles in 2021, 2022, and 2023;
 154 respectively. The relationship between multi-year AOD_{500 nm} and AE_{440-870 nm} illustrates that fine mode
 155 particles are primarily concentrated in the range of AOD_{500 nm} < 0.1, while high AOD_{500 nm} values, which
 156 occur occasionally, are caused by coarse mode particles (Fig. 2b). Although fine mode particles have a
 157 longer suspension time in the atmosphere and can efficiently scatter and absorb sunlight, leading to lower
 158 AOD ranges, it is worth mentioning that in the coastal regions of Antarctica, the dominant role in AOD
 159 is sometimes played by coarse mode particles. These particles, with larger radii and higher volume
 160 concentrations, originate mainly from abundant sea salt sources. Their presence results in increased
 161 scattering and absorption of sunlight, emphasizing the significance of coarse mode particles in
 162 determining AOD levels in the Antarctic coastal areas (Su et al., 2022)



163
 164 **Figure 2 (a) Monthly variation of mean aerosol optical depth at different wavelengths measured over**
 165 **Zhongshan Station in Antarctica from 2020 to 2023. (b) Relationship between AOD_{500 nm} and AE_{440-870 nm} over**
 166 **Zhongshan Station from 2020 to 2023.**

167 **Table 1 Annual mean and standard deviation of aerosol optical depth at different wavelengths and Angstrom**
 168 **Exponent at 440-870 nm at Zhongshan Station from 2020 to 2023.**

	2020	2021	2022	2023
AOD _{1640 nm}	0.02811 \pm 0.10243	0.02639 \pm 0.07887	0.04989 \pm 0.14113	0.01604 \pm 0.03631
AOD _{1020 nm}	0.04898 \pm 0.09501	0.04519 \pm 0.0728	0.06709 \pm 0.13069	0.03965 \pm 0.0337

AOD_{870 nm}	0.04659±0.09314	0.03901±0.07044	0.06033±0.1264	0.03669±0.03244
AOD_{675 nm}	0.05887±0.09128	0.04224±0.06786	0.06339±0.12164	0.04407±0.03139
AOD_{500 nm}	0.07431±0.08972	0.05083±0.06557	0.07108±0.1173	0.05288±0.03091
AOD_{440 nm}	0.08093±0.08902	0.05744±0.0648	0.07715±0.11592	0.0574±0.03106
AOD_{380 nm}	0.08854±0.09143	0.06302±0.06542	0.07699±0.11697	0.0613±0.03169
AOD_{340 nm}	0.08758±0.09536	0.05881±0.06431	0.0732±0.11763	0.05831±0.03242
AE_{440-870 nm}	1.13411±0.41069	0.95284±0.33823	0.88293±0.3738	0.75257±0.20645

169

	<u>2020</u>	<u>2021</u>	<u>2022</u>	<u>2023</u>
<u>AOD_{1640 nm}</u>	<u>0.028±0.102</u>	<u>0.026±0.079</u>	<u>0.050±0.141</u>	<u>0.016±0.036</u>
<u>AOD_{1020 nm}</u>	<u>0.049±0.095</u>	<u>0.045±0.073</u>	<u>0.067±0.131</u>	<u>0.040±0.034</u>
<u>AOD_{870 nm}</u>	<u>0.047±0.093</u>	<u>0.039±0.070</u>	<u>0.060±0.126</u>	<u>0.037±0.032</u>
<u>AOD_{675 nm}</u>	<u>0.059±0.091</u>	<u>0.042±0.068</u>	<u>0.063±0.122</u>	<u>0.044±0.031</u>
<u>AOD_{500 nm}</u>	<u>0.074±0.090</u>	<u>0.051±0.066</u>	<u>0.071±0.117</u>	<u>0.053±0.031</u>
<u>AOD_{440 nm}</u>	<u>0.081±0.089</u>	<u>0.057±0.065</u>	<u>0.077±0.116</u>	<u>0.057±0.031</u>
<u>AOD_{380 nm}</u>	<u>0.089±0.091</u>	<u>0.063±0.065</u>	<u>0.077±0.117</u>	<u>0.061±0.032</u>
<u>AOD_{340 nm}</u>	<u>0.088±0.095</u>	<u>0.059±0.064</u>	<u>0.073±0.118</u>	<u>0.058±0.032</u>
<u>AE_{440-870 nm}</u>	<u>1.134±0.411</u>	<u>0.953±0.338</u>	<u>0.883±0.374</u>	<u>0.753±0.206</u>

170

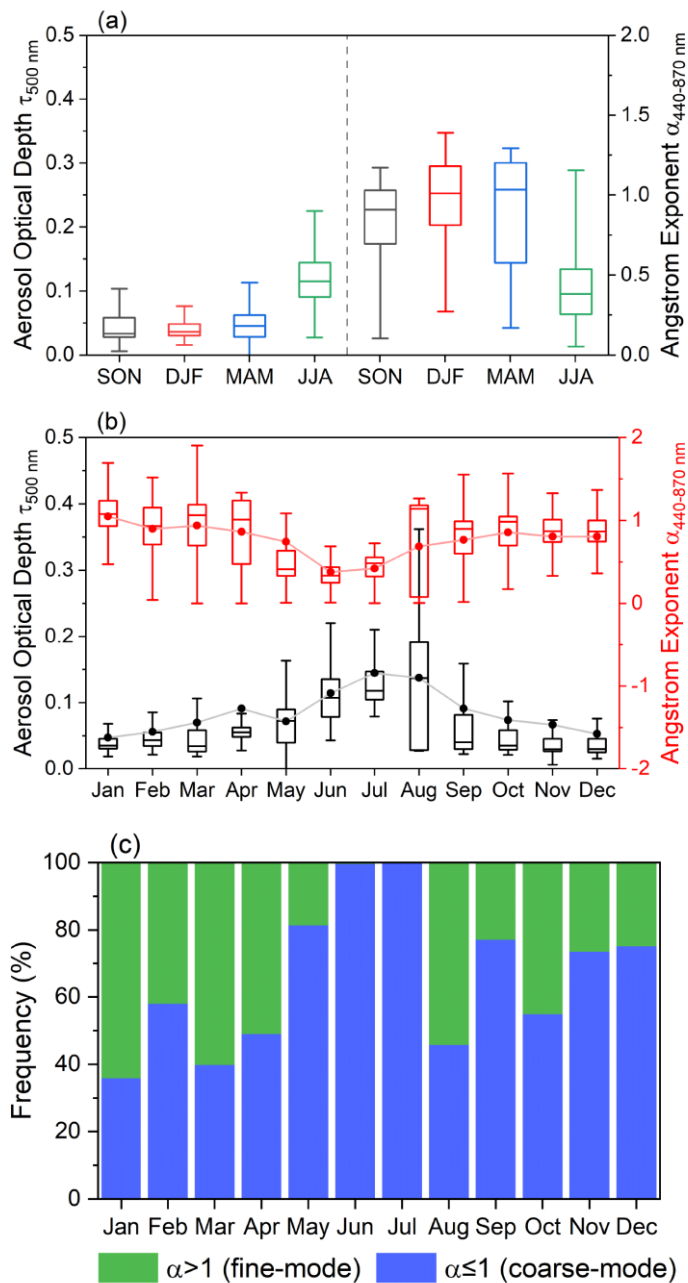
171 **0363.2 Seasonal and Monthly Variations in AOD and Ångström Exponent**

172 The seasonal variation of AOD_{500 nm} and AE_{440-870 nm} over Zhongshan Station suggests the median AOD₅₀₀
173 nm values are lower in spring (0.033), summer (0.036), and autumn (0.045), but higher in winter (0.115),
174 while the AE_{440-870 nm} values are 0.908, 1.010, 1.036, and 0.381, respectively (Fig. 3a). The frequency
175 histograms show that the highest frequency range of AOD_{500 nm} is 0.02 to 0.04 in spring, summer, and
176 autumn, while 0.08 to 0.12 in winter (Fig. S2). The normal fitting curves of the frequency histograms of
177 AE_{440-870 nm} indicate that the peak in winter is in the low-value range (0.3~0.4), while the peaks in spring,
178 summer, and autumn are in the high-value range (1.0~1.2).

179 The seasonal variations in AOD and AE are consistent with previous findings on sea salt aerosol
180 concentrations, although the mechanism behind this seasonal variation is multifaceted. Wang and Huang
181 et al. have indicated that higher winter wind speeds at Zhongshan Station can elevate marine source
182 aerosol concentrations, primarily composed of sea salt, potentially explaining the winter peak in sea salt
183 concentration (Hong et al., 2009; Huang et al., 2005). However, Hall and Wolff propose that the high
184 sea salt load correlates more with moderate wind speeds and shifts in wind direction, rather than high
185 wind speeds, with concentrated brine on freshly formed ice surfaces acting as a source of winter sea salt
186 (Hall and Wolff, 1998). Moreover, blowing snow over sea ice generates aerosols primarily made of sea
187 salt, contributing to the winter peak in sea salt aerosols (Frey et al., 2020). ~~In summer, Lower~~ sea salt
188 concentrations ~~in summer determined~~ lead to lower ~~background levels of AOD levels,~~ ~~but the effect of~~
189 ~~enhanced marine biogenic emissions on AOD may increase~~ and the higher AE indicates a dominance of
190 ~~smaller particle sizes~~. In the marine boundary layer over the eastern Southern Ocean sector, $nssS_4^{2-}$
191 and MSA contribute approximately 40% of the total mass of fine aerosols (particle size $< 0.56 \mu m$) (Xu
192 et al., 2021). Xu et al. reported the annual mean concentrations of $nssS_4^{2-}$ and MSA at Zhongshan
193 Station were $0\text{-}79 \text{ ng m}^{-3}$ and $19\text{-}41 \text{ ng m}^{-3}$, respectively, with the maximum concentrations were
194 observed in summer (Xu et al., 2019). This increase in summer concentrations is attributed to enhanced
195 solar radiation, phytoplankton blooms in the polynyas releasing DMS (Zhang et al., 2015), and the DMS
196 in the atmosphere is oxidized by radicals such as O_3 (significant at high latitudes), OH, and BrO in the
197 gas phase (Boucher et al., 2003), resulting in elevated concentrations of MSA and $nssS_4^{2-}$. The positive
198 correlation between mean surface chlorophyll and AOD in the Southern Ocean confirmed the
199 contribution of DMS flux to aerosol load during summer (Gabric et al., 2005).

200 The monthly variations in $AOD_{500 \text{ nm}}$ and $AE_{440\text{-}870 \text{ nm}}$ at Zhongshan Station suggest an opposite trend,
201 with the mean values of $AOD_{500 \text{ nm}}$ peaking in July and $AE_{440\text{-}870 \text{ nm}}$ reaching its lowest in June (Fig. 3b).
202 Median $AOD_{500 \text{ nm}}$ values increase slightly from January to February, followed by a decrease in March
203 and increase continuously from March to August, reach the maximum value, then gradually decrease,
204 and reach the minimum in November and December. The percentages of $AE_{440\text{-}870 \text{ nm}} > 1.0$ and $AE_{440\text{-}870 \text{ nm}}$
205 < 1.0 represent the proportion of the monthly occurrence frequency of fine and coarse mode particles
206 (Fig. 3c). The monthly mean and median $AOD_{500 \text{ nm}}$ values are consistent with the proportion of coarse

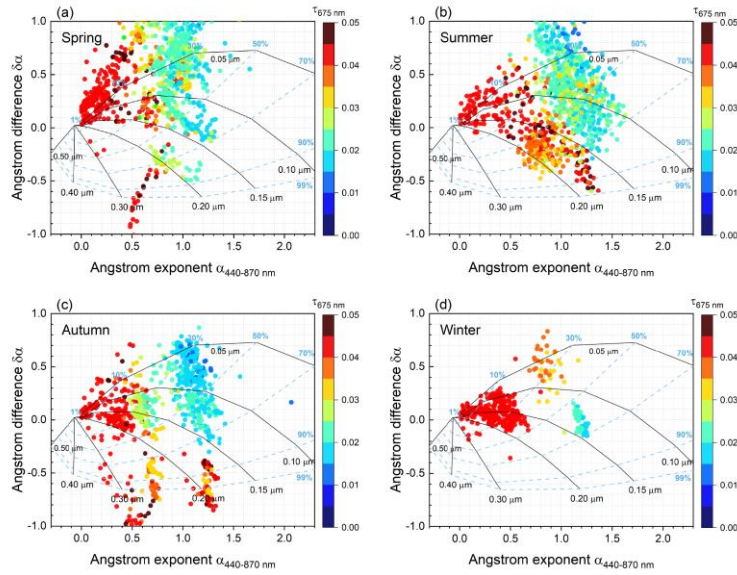
207 mode particles ($AE_{440-870 \text{ nm}} > 1.0$), suggesting that the variation characteristics of $AOD_{500 \text{ nm}}$ at
 208 Zhongshan Station are primarily influenced by coarse mode particles. Given that Zhongshan Station is
 209 located in the coastal area of Antarctica, it is suspected that these coarse particles may be sea salt aerosols.



210
 211 **Figure 3 (a)** Seasonal variation of aerosol optical depth at 500 nm and Angstrom exponent at 440-870 nm over
 212 Zhongshan Station. For each monthly box, the central line indicates the median; and the bottom and top edges
 213 of the box indicate the 25th and 75th percentiles, respectively. **(b)** Variations in monthly $AOD_{500 \text{ nm}}$ and AE_{440-}
 214 870 nm at Zhongshan Station. For each monthly box, the central line indicates the median; the dot represents
 215 the mean; and the bottom and top edges of the box indicate the 25th and 75th percentiles, respectively. **(c)**
 216 Monthly percentages of Ångström exponent >1.0 (green) and Ångström exponent ≤ 1.0 (blue) at Zhongshan
 217 Station from 2020 to 2023.

218 Additionally, we used a graphical method proposed by Gobbi et al (Gobbi et al., 2007), which is based
219 on Mie calculation and correlates Ångström exponent (α) and Ångström exponent spectral difference
220 ($\delta\alpha$) with fine mode aerosol effective radius (R_{eff}) and fine mode fraction to investigate the aerosol
221 modification processes at Zhongshan Station in different seasons. Figure 4 presents a schematic diagram
222 of the classification of aerosol types using the α and $\delta\alpha$ functions of a dual-mode, lognormal
223 distribution with refractive index = $1.4 - 0.001i$ as reference. It is known from Jurányi and Weller'
224 research that the refractive index of Antarctic coastal aerosol is about 1.4, so it seems reasonable to use
225 this reference (Jurányi and Weller, 2019). We utilized AOD_{440nm} , AOD_{675nm} , and AOD_{870nm} to calculate
226 $\alpha_{440-675nm}$, $\alpha_{440-870nm}$, and $\alpha_{675-870nm}$, and then get the $\delta\alpha = \alpha_{440-675nm} - \alpha_{675-870nm}$. The
227 negative values of $\delta\alpha$ indicate the dominance of fine mode aerosol, while positive values indicate the
228 effect of two separate particle modes (Kaufman, 1993). The solid black line represents the size of fine
229 mode particles (R_{eff}), and the dashed blue line represents the proportion of the contribution of fine mode
230 particles to AOD (η). In Fig. 4, increasing AOD_{675nm} is associated with the declining η (spring and
231 winter) and increasing R_{eff} (summer and autumn). This indicates that higher aerosol loads in spring and
232 winter are attributed to increased coarse-mode particle fractions, whereas in summer and autumn are
233 primarily associated with the increase of fine-mode particle size. Previous studies have indicated that sea
234 salt dominates winter aerosols in the coastal areas of Antarctica (Hall and Wolff, 1998; Weller et al.,
235 2008), and Xu et al observed that the highest mean concentration of sea salt in September at Zhongshan
236 Station, these can explain the $\delta\alpha$ values are mainly positive in spring and winter, and η is concentrated
237 within the range of less than 50% (Xu et al., 2019). In summer and autumn, apart from common sea salt
238 aerosols ($\delta\alpha > 0$, $\eta < 50$), the high AOD is mainly related to the particle growth such as hygroscopic
239 growth or condensation of fine mode aerosols ($R_{eff}: 0.10\mu m \sim 0.20\mu m$). This may be linked to the
240 atmospheric oxidation of (DMS) emitted by biological sources in coastal regions, or the aging process
241 of aerosols originating from other sources, as the rate of new particle formation and particulate matter
242 growth in summer is much greater than in winter in the Antarctica (Davison et al., 1996; Lachlan-Cope
243 et al., 2020; Weller et al., 2015).

244

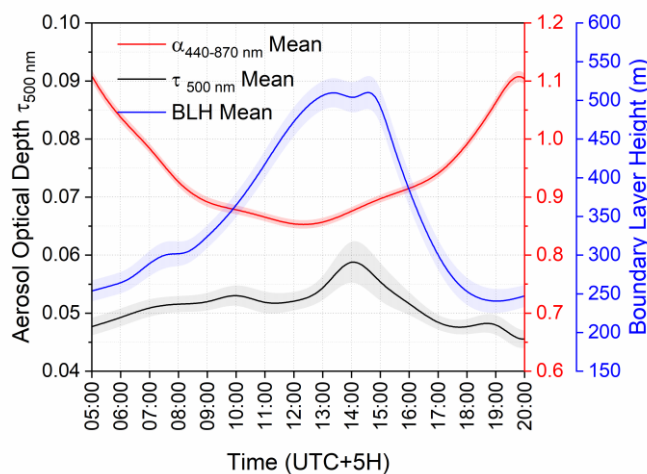


245
 246 **Figure 4** Ångström exponent difference ($\delta\alpha = \alpha_{440-675\text{ nm}} - \alpha_{675-870\text{ nm}}$) as a function of the $\alpha_{440-870\text{ nm}}$
 247 and $\text{AOD}_{675\text{ nm}}$ (colour scale) during (a) spring, (b) summer, (c) autumn, and (d) winter at Zhongshan Station.
 248 The black lines indicate the R_{eff} of fine-mode aerosols, while the blue lines correspond to fine-mode fraction
 249 (η).

250 3.3 Relationship between AOD, Ångström Exponent and Meteorological Conditions

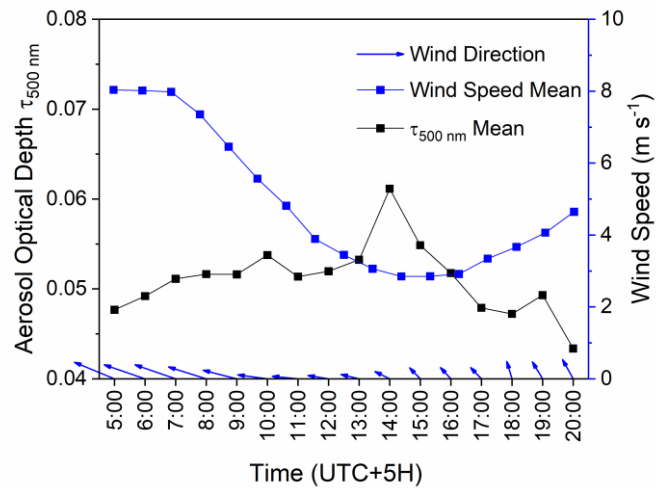
251 In this section, we analyse the diurnal variation characteristics of $\text{AOD}_{500\text{ nm}}$ and $\text{AE}_{440-870\text{ nm}}$ during
 252 summer and explore their correlation with meteorological variables within the planetary boundary layer
 253 (PBL), such as wind directions and speeds, temperature, and relative humidity. We calculated the diurnal
 254 variations of $\text{AOD}_{500\text{ nm}}$ and $\text{AE}_{440-870\text{ nm}}$ based on observations collected at Zhongshan Station during
 255 summer (December-February, 2020-2023), with each hourly mean containing at least one thousand
 256 individual observations (Fig. 5 **Figure 5**). The mean $\text{AOD}_{500\text{ nm}}$ exhibited an increase from 5:00 to 14:00
 257 (local time of Zhongshan Station), reaching a maximum value (0.06 ± 0.04), and then decreased. The
 258 mean $\text{AE}_{440-870\text{ nm}}$ decreased from 5:00 to 12:00, ~~to-reaching~~ the lowest value (0.85 ± 0.25), and then
 259 increased. These results indicate that the highest aerosol load occurs at 14:00, accompanied by a larger
 260 aerosol particle size during this period. The diurnal variation of boundary layer height (BLH) is almost
 261 consistent with the variation of $\text{AOD}_{500\text{ nm}}$, which is inconsistent with the general conclusion that the
 262 negative correlation between BLH and particulate matter concentration in the mid-latitudes (Lou et al.,
 263 2019; Miao and Liu, 2019). However, a minor decline in BLH is noticeable when the $\text{AOD}_{500\text{ nm}}$ value
 264 reaches its peak at 14:00. Consequently, we suspect that the weak absorption and low content of Antarctic

265 aerosols typically do not suffice to form an “aerosol-boundary layer” positive feedback mechanism, but
 266 may contribute to reducing the BLH when AOD is high (Lou et al., 2019; Petäjä et al., 2016).



267
 268 **Figure 5 Diurnal variation of AOD_{500 nm} and AE_{440-870 nm} at Zhongshan Station. The black line indicates the**
 269 **mean of AOD_{500 nm}; the red line represents the mean of AE_{440-870 nm}; the blue line represents the mean of BLH.**
 270 **The shadow represents the standard deviation of the mean.**

271 Moreover, the diurnal variation of the 2-minute wind at Zhongshan Station reveals prevailing southeast
 272 direction, with average speeds ranging from 2 to 9 m s⁻¹. There is a noticeable decline in wind speeds
 273 between 5:00 and 14:00, followed by a gradual increase thereafter (Fig. 6). Given that the CE318-T is
 274 positioned westward of the main Zhongshan Station building, the eastward winds may carry emissions
 275 originating from western stations such as Zhongshan and Progress Station. The relationship between the
 276 diurnal variation of AOD_{500 nm} and wind speed is more obvious: AOD_{500 nm} exhibits a decline (increase)
 277 concurrent with decreasing (increasing) wind speeds. This correlation stems from the fact that higher
 278 wind speeds facilitate the dispersion of pollutants, leading to a reduction in AOD, and vice versa (Coccia,
 279 2021; Liu et al., 2020; Wang et al., 2022).



280

281 **Figure 6 Diurnal variations of 2-minute wind direction and speed, and AOD_{500 nm} in summer at Zhongshan**
 282 **Station.**

283 The influence of temperature and relative humidity on aerosol parameters is relatively complex.

284 Temperature affects aerosol particle concentration by influencing the air convection and influences

285 the formation and optical properties of secondary by controlling chemical transformation (Han et al.,

286 2007; Li et al., 2020). Relative humidity affects the chemical composition, size distribution, and optical

287 properties of aerosol particles by affecting their aqueous-phase reactions and gas-particle partitioning

288 (Altieri et al., 2008; Ding et al., 2021; Hennigan et al., 2008; Sun et al., 2013). The diurnal variations of

289 AOD_{500 nm}, temperature, and relative humidity in summer at Zhongshan Station show that AOD_{500 nm} is

290 positively correlated with temperature with a correlation coefficient of 0.22, and AOD_{500 nm} is negatively

291 correlated with relative humidity with a correlation coefficient of -0.59 (Fig. 7). This indicates that rising

292 (declining) temperature and declining (rising) relative humidity during the day may contribute to an

293 increase (declining) in aerosol load. Previous studies have shown a positive correlation between

294 temperature and AOD (Basharat et al., 2023). During the summer at Zhongshan Station, high

295 temperatures may destroy the physical properties of bare rocks and promote the formation and diffusion

296 of particulate matter, thereby increasing the aerosol load (Zhang, 2024). However, there is a study

297 showing that higher temperatures may reduce methane sulfinic acid (MSIA) yield (Cecilia Arsene et al.,

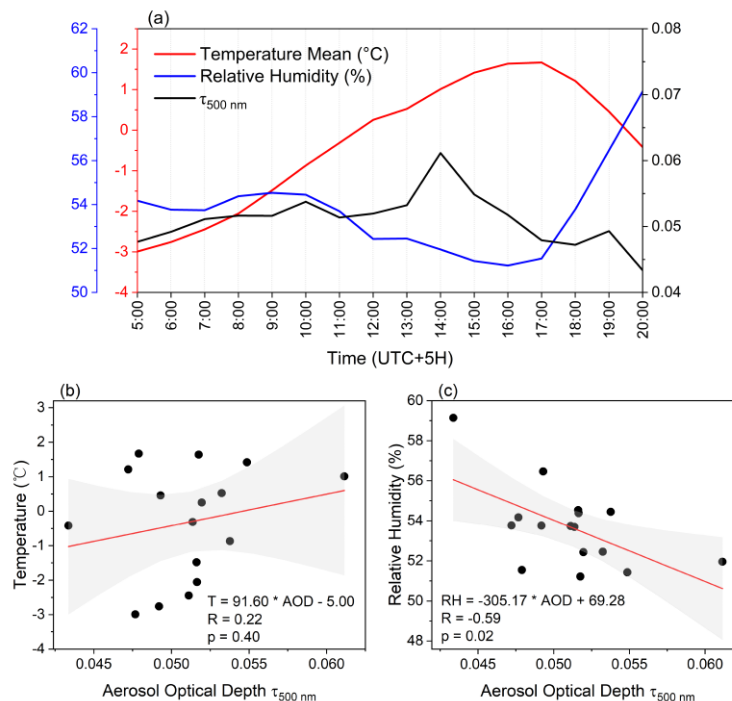
298 1999). Therefore, the effect of temperature on the AOD at Zhongshan Station is complex, resulting in an

299 insignificant positive correlation. The relationship between relative humidity and AOD is inconclusive

300 (Gautam et al., 2022), as high relative humidity may contribute to the increase of aerosol hygroscopic

301 properties leading to an increase in AOD (Meng et al., 2024), or it may contribute to a decrease in AOD

302 by reducing dust particles in the air (Zhang, 2024). Therefore, the influence of temperature and relative
 303 humidity on AOD may be related to the physicochemical properties of local aerosols and their sourcing
 304 and sink processes.



305
 306 **Figure 7 (a) Diurnal variations of AOD_{500 nm} (black), temperature (red), and relative humidity (blue) in**
 307 **summer at Zhongshan Station; (b) relationship between AOD_{500 nm} and temperature; and (c) relationship**
 308 **between AOD_{500 nm} and relative humidity. The red line indicates the regression line obtained by fitting a linear**
 309 **regression, and the grey bands indicate the confidence intervals for the linear regression.**

310 4 Discussion

311 4.1 Potential effects of aerosol sources on AOD levels

312 Besides meteorological conditions, aerosol sources may also influence the diurnal variation
 313 characteristics of AOD.~~In addition to meteorological conditions that can affect the diurnal variation~~
 314 ~~characteristics of AOD, we believe that aerosol sources may be another influencing factor.~~ We classified
 315 days with mean AOD below the 5th percentile as low AOD day and those above the 95th percentile as
 316 high AOD day (Fig. S3 and Table S1). Using the HYSPLIT backward trajectory model, we found that
 317 air masses on high AOD days primarily originated from the ocean, whereas those on low AOD days
 318 mostly came from the interior of Antarctica (Fig. S4). The altitudes of the backward trajectories show
 319 that during low AOD days, the air mass originating from the ocean usually starts at a lower altitude

320 (<1000 m), rises to a higher altitude (~2000 m) and then descends to Zhongshan Station (2020-05-15
321 and 2020-12-25), while the air mass originating from the interior of Antarctica usually starts at a higher
322 altitude (~3000 m) and then descends to Zhongshan Station. This indicates that particles from the
323 Antarctic plateau or the free troposphere above the Antarctic interior are transported to Zhongshan
324 Station by katabatic winds. Researches show that the katabatic winds driven by latent cooling occurring
325 in the high-wind East Antarctic can rush the dense air from the interior plateau to the coast (Simmons et
326 al., 2021; Yu et al., 2020). Combined with the AE values, we can find that the AE values of low AOD
327 days are usually greater than 1, indicating the small particle size, thus, we suspect that these fine particles
328 may be $nssSO_4^{2-}$ from the Antarctic interior (Pei et al., 2021). In contrast, in high AOD days, the air
329 mass all originates in the ocean and usually starts at a lower altitude. The AE values corresponding to
330 high AOD moment on high AOD days are extremely low (<0.5), indicating that the particle size is large,
331 thus, we suspect that these aerosols may consist of coarse sea salt particles.

332 **4.2 Potential effects of aerosol particles on cloud and radiative forcing**

333 The optical properties of aerosols play a crucial role in their impact on radiative forcing, cloud formation,
334 and local climate. In our analysis of the variations in AOD and AE, we provided insights into the aerosol
335 loading, particle sizes, and possible formation and growth mechanisms in the atmosphere over
336 Zhongshan Station. During winter and spring, coarse mode particles are predominantly derived from sea
337 salt. Studies have shown that aerosols larger than 0.13 μm in the marine boundary layer contain sea salt,
338 contributing to most of the aerosol scattering and inducing cooling effects (Murphy et al., 1998).
339 Additionally, the size and inhomogeneity of sea salt particles are often associated with relative humidity.
340 Compared to remote oceans, the low relative humidity in coastal Antarctica may introduce more
341 inhomogeneous sea salt particles, resulting in up to a 12% change in direct radiative forcing due to
342 inhomogeneity (Wang et al., 2019).
343 However, we are particularly interested in the behaviour of aerosol particles during summer since solar
344 radiation is limited in winter. In summer and autumn, the increase in fine mode particles is closely related
345 to the release of biogenic aerosols, such as DMS, emitted by phytoplankton in the marginal ice zone.
346 When particles grow to a size suitable for cloud condensation nuclei or ice nucleating particles, they can
347 affect the formation of low-level mixed-phase clouds in coastal areas, contributing to the formation of

348 low-level ice clouds. At the same time, the increased number density of cloud droplets enhances cloud
349 reflectivity, resulting in negative radiative forcing (Satheesh and Krishna Moorthy, 2005). A recent study
350 revealed that in the shallow mixed-phase clouds over Antarctica, the concentrations of cloud-relevant
351 aerosol particles match the concentrations of ice crystals and cloud droplets (Radenz et al., 2024). the
352 number of particles plays a crucial role in cloud growth. Increasing particle concentration results in a
353 higher abundance of liquid droplets and ice crystals within clouds, which can impact cloud lifespan and
354 potentially influence local weather and climate. Therefore, continuous monitoring of aerosol optical
355 properties in coastal Antarctica is vital to improve our comprehension of aerosol radiative forcing
356 variations caused by changes in aerosol loading and particle size.

357 **5 Summary**

358 This study analysed the AOD and AE variations retrieved from CE318-T sun photometer data spanning
359 from January 2020 to April 2023 at Zhongshan Station in Antarctica. The main conclusions we draw are
360 as follows:

361 At Zhongshan Station, AOD at Zhongshan Station varied from ranged from 0.00 to 0.20, Fine mode
362 particles were predominantly found in the lower AOD range, while higher AOD values were mainly
363 attributed to coarse mode particles, with fine mode particles concentrated in the low AOD range, and high
364 AOD attributed to coarse mode particles.

365 Seasonally, AOD exhibited a pattern of lower values in summer and higher values in winter, and the AE
366 displayed an opposite trend. The increases in AOD during summer and autumn may be linked to particle
367 growth, whereas the increases during spring and winter are associated with a decline in the fraction of
368 fine mode particles. AOD showed seasonal characteristics of low in summer, and high in winter, while
369 AE showed the opposite. From spring to autumn, aerosols are dominated by fine particles, as retreating
370 sea ice provides suitable conditions for phytoplankton blooms (Lizotte, 2001). In winter, the increase in
371 sea salt dominated the increase in AOD and caused low AE levels. Additionally, summer and autumn
372 AOD increases are possibly linked to particle growth, while spring and winter increases are associated
373 with fine mode fraction decline.

374 Low aerosol load over Zhongshan Station was not enough to form an “aerosol-boundary layer” positive
375 feedback mechanism, but the slight decrease in BLH may be related to AOD diurnal peak at 14:00.
376 Moreover, high (low) wind speeds facilitated pollutant dispersion (accumulation), leading to reduced
377 (increased) AOD. A weak positive correlation was noted between temperature and AOD ($R = 0.22$, $p =$
378 0.40), and a negative correlation between relative humidity and AOD ($R = -0.59$, $p = 0.02$). The
379 mechanisms underlying temperature and humidity's influence on aerosols remain unclear, possibly
380 linked to local aerosol properties at Zhongshan Station. In addition, we discuss the influence of aerosol
381 sources on AOD. The backward trajectories show that the air masses on high AOD days come from the
382 ocean, and the low AE values indicate that the particle size is larger, we speculate that the main
383 composition of the aerosols is sea salt. The air masses on the low AOD days mainly come from the
384 interior of Antarctica, and the high AE values indicate that the particle size is small. We speculate that
385 the katabatic winds rush the air from the Antarctic plateau to Zhongshan Station.

386 **Data availability**

387 The data included in this study can be accessed via <https://zenodo.org/records/10983098>. Boundary layer
388 height data downloaded from ECMWF ERA5 ([https://www.ecmwf.int/en/forecasts/dataset/ecmwf-](https://www.ecmwf.int/en/forecasts/dataset/ecmwf-reanalysis-v5)
389 [reanalysis-v5](https://www.ecmwf.int/en/forecasts/dataset/ecmwf-reanalysis-v5)). Backward trajectory of air mass and the meteorological data are obtained from NOAA
390 Air Resources Laboratory (https://www.ready.noaa.gov/HYSPLIT_traj.php).

391 **Author contributions**

392 The paper is a result of the lead author's research work under the supervision of MD, LZ, YS. ZZ and
393 YZ provided constructive comments. MD, QW and BT provided experimental data. ZL provided aerial
394 photos of Zhongshan Station. LC wrote the first draft of the paper with the help and support of all the
395 authors. [HC provided guidance for the manuscript revisions.](#)

396 **Competing interests**

397 The contact author has declared that none of the authors has any competing interests.

398 **Acknowledgments**

399 Funding for this study was provided by the National Natural Science Foundation of China (42122047),
400 the National Key Research and Development Program of China (2021YFC2802504), and the Basic
401 Research Fund of the Chinese Academy of Meteorological Science (2023Z015&2023Z025).

402 **Reference**

403 Alghoul, M., Khamies, H., Assadeg, J., Yahya, M., Alfegi, E., and Sopian, K.:
404 Impact of Aerosol Optical Depth on Solar Radiation Budget, in: Proceedings of the 3rd
405 World Scientific and Engineering Academy and Society Int., Conference on renewable
406 energy sources, 2009.

407 Altieri, K. E., Seitzinger, S. P., Carlton, A. G., Turpin, B. J., Klein, G. C., and
408 Marshall, A. G.: Oligomers formed through in-cloud methylglyoxal reactions:
409 Chemical composition, properties, and mechanisms investigated by ultra-high
410 resolution FT-ICR mass spectrometry, *Atmospheric Environment*, 42, 1476–1490,
411 <https://doi.org/10.1016/j.atmosenv.2007.11.015>, 2008.

412 Barreto, Á., Cuevas, E., Granados-Muñoz, M.-J., Alados-Arboledas, L., Romero,
413 P. M., Gröbner, J., Kouremeti, N., Almansa, A. F., Stone, T., Toledano, C., Román, R.,
414 Sorokin, M., Holben, B., Canini, M., and Yela, M.: The new sun-sky-lunar Cimel
415 CE318-T multiband photometer - a comprehensive performance evaluation,
416 *Atmospheric Measurement Techniques*, 9, 631–654, [https://doi.org/10.5194/amt-9-](https://doi.org/10.5194/amt-9-631-2016)
417 631-2016, 2016.

418 Basharat, U., Tariq, S., Chaudhry, M. N., Khan, M., Bonah Agyekum, E., Fendzi
419 Mbasso, W., and Kamel, S.: Seasonal correlation of aerosols with soil moisture,
420 evapotranspiration, and vegetation over Pakistan using remote sensing, *Heliyon*, 9,
421 e20635, <https://doi.org/10.1016/j.heliyon.2023.e20635>, 2023.

422 Boucher, O., Moulin, C., Belviso, S., Aumont, O., Bopp, L., Cosme, E., von
423 Kuhlmann, R., Lawrence, M. G., Pham, M., Reddy, M. S., Sciare, J., and Venkataraman,
424 C.: DMS atmospheric concentrations and sulphate aerosol indirect radiative forcing: a
425 sensitivity study to the DMS source representation and oxidation, *Atmospheric*
426 *Chemistry and Physics*, 3, 49–65, <https://doi.org/10.5194/acp-3-49-2003>, 2003.

427 Cecilia Arsene, Barnes, I., and Becker, K. H.: FT-IR product study of the photo-
428 oxidation of dimethyl sulfide: Temperature and O₂ partial pressure dependence,
429 *Physical Chemistry Chemical Physics*, 1, 5463–5470,
430 <https://doi.org/10.1039/A907211J>, 1999.

431 Che, H., Xia, X., Zhao, H., Li, L., Gui, K., Zheng, Y., Song, J., Qi, B., Zhu, J.,

432 Miao, Y., Wang, Y., Wang, Z., Wang, H., Dubovik, O., Holben, B., Chen, H., Shi, G.,
433 and Zhang, X.: Aerosol optical and radiative properties and their environmental effects
434 in China: A review, *Earth-Science Reviews*, 248, 104634,
435 <https://doi.org/10.1016/j.earscirev.2023.104634>, 2024.

436 Coccia, M.: How do low wind speeds and high levels of air pollution support the
437 spread of COVID-19?, *Atmos Pollut Res*, 12, 437–445,
438 <https://doi.org/10.1016/j.apr.2020.10.002>, 2021.

439 Davison, B., O’dowd, C., Hewitt, C. N., Smith, M. H., Harrison, R. M., Peel, D.
440 A., Wolf, E., Mulvaney, R., Schwikowski, M., and Baltenspergert, U.: Dimethyl sulfide
441 and its oxidation products in the atmosphere of the Atlantic and Southern Oceans,
442 *Atmospheric Environment*, 30, 1895–1906, [https://doi.org/10.1016/1352-2310\(95\)00428-9](https://doi.org/10.1016/1352-2310(95)00428-9), 1996.

444 Ding, J., Dai, Q., Zhang, Y., Xu, J., Huangfu, Y., and Feng, Y.: Air humidity affects
445 secondary aerosol formation in different pathways, *Science of The Total Environment*,
446 759, 143540, <https://doi.org/10.1016/j.scitotenv.2020.143540>, 2021.

447 Ding, M., Zou, X., Sun, Q., Yang, D., Zhang, W., Bian, L., Lu, C., Allison, I., Heil,
448 P., and Xiao, C.: The PANDA automatic weather station network between the coast and
449 Dome A, East Antarctica, *Earth System Science Data*, 14, 5019–5035,
450 <https://doi.org/10.5194/essd-14-5019-2022>, 2022.

451 Frey, M. M., Norris, S. J., Brooks, I. M., Anderson, P. S., Nishimura, K., Yang, X.,
452 Jones, A. E., Nerentorp Mastromonaco, M. G., Jones, D. H., and Wolff, E. W.: First
453 direct observation of sea salt aerosol production from blowing snow above sea ice,
454 *Atmospheric Chemistry and Physics*, 20, 2549–2578, <https://doi.org/10.5194/acp-20-2549-2020>, 2020.

456 Gabric, A. J., Shephard, J. M., Knight, J. M., Jones, G., and Trevena, A. J.:
457 Correlations between the satellite-derived seasonal cycles of phytoplankton biomass
458 and aerosol optical depth in the Southern Ocean: Evidence for the influence of sea ice,
459 *Global Biogeochemical Cycles*, 19, <https://doi.org/10.1029/2005GB002546>, 2005.

460 Gadhavi, H. and Achuthan, J.: Aerosol characteristics and aerosol radiative forcing
461 over Maitri, Antarctica, *Current Science*, 86, 296, 2004.

462 Gautam, S., Elizabeth, J., Gautam, A. S., Singh, K., and Abhilash, P.: Impact
463 Assessment of Aerosol Optical Depth on Rainfall in Indian Rural Areas, *Aerosol
464 Science and Engineering*, 6, 186–196, <https://doi.org/10.1007/s41810-022-00134-9>,
465 2022.

466 Gobbi, G. P., Kaufman, Y. J., Koren, I., and Eck, T. F.: Classification of aerosol
467 properties derived from AERONET direct sun data, *Atmospheric Chemistry and*

468 Physics, 7, 453–458, <https://doi.org/10.5194/acp-7-453-2007>, 2007.

469 Hall, J. S. and Wolff, E. W.: Causes of seasonal and daily variations in aerosol sea-
470 salt concentrations at a coastal Antarctic station, *Atmospheric Environment*, 32, 3669–
471 3677, [https://doi.org/10.1016/S1352-2310\(98\)00090-9](https://doi.org/10.1016/S1352-2310(98)00090-9), 1998.

472 Han, D., Liu, W., Zhang, Y., Lu, Y., Liu, J., and Zhao, N.: Influence of temperature
473 and relative humidity upon aerosol mass concentrations vertical distributions, *Journal*
474 *of University of Chinese Academy of Sciences*, 24, 619,
475 <https://doi.org/10.7523/j.issn.2095-6134.2007.5.011>, 2007.

476 Harder, S., Warren, S. G., and Charlson, R. J.: Sulfate in air and snow at the South
477 Pole: Implications for transport and deposition at sites with low snow accumulation,
478 *Journal of Geophysical Research: Atmospheres*, 105, 22825–22832,
479 <https://doi.org/10.1029/2000JD900351>, 2000.

480 Hennigan, C. J., Bergin, M. H., Dibb, J. E., and Weber, R. J.: Enhanced secondary
481 organic aerosol formation due to water uptake by fine particles, *Geophysical Research*
482 *Letters*, 35, <https://doi.org/10.1029/2008GL035046>, 2008.

483 Hong, J., Chen, L., and Yang, X.: Characteristics of the aerosols in Zhongshan
484 Station, Antarctica (in Chinese), *Chinese Journal of Polar Research*, 21, 1, 2009.

485 Huang, Z., Ji, W., Yang, X., Huang, R., Tang, R., Yu, T., and Zhang, G.: The
486 chemical composition of marine aerosol over Zhongshan Station in Antarctica and its
487 sources discrimination in 1998 (in Chinese), *Acta Oceanologica Sinica*, 27, 59–66,
488 2005.

489 Jurányi, Z. and Weller, R.: One year of aerosol refractive index measurement from
490 a coastal Antarctic site, *Atmospheric Chemistry and Physics*, 19, 14417–14430,
491 <https://doi.org/10.5194/acp-19-14417-2019>, 2019.

492 Kamra, V. P., Devendraa Siingh, A. K.: Antarctic Aerosols and Climate:
493 Measurements at a Coastal Antarctic Station, in: *Climate Variability of Southern High*
494 *Latitude Regions*, CRC Press, 2022.

495 Kang, S., Zhang, Y., Qian, Y., and Wang, H.: A review of black carbon in snow
496 and ice and its impact on the cryosphere, *Earth-Science Reviews*, 210, 103346,
497 <https://doi.org/10.1016/j.earscirev.2020.103346>, 2020.

498 Kannemadugu, H. B. S., Sudhakaran Syamala, P., Taori, A., Bothale, R. V., and
499 Chauhan, P.: Atmospheric aerosol optical properties and trends over Antarctica using
500 in-situ measurements and MERRA-2 aerosol products, *Polar Science*, 38, 101011,
501 <https://doi.org/10.1016/j.polar.2023.101011>, 2023.

502 Kaufman, Y. J.: Aerosol optical thickness and atmospheric path radiance, Journal
503 of Geophysical Research: Atmospheres, 98, 2677–2692,
504 <https://doi.org/10.1029/92JD02427>, 1993.

505 Lachlan-Cope, T., Beddows, D. C. S., Brough, N., Jones, A. E., Harrison, R. M.,
506 Lupi, A., Yoon, Y. J., Virkkula, A., and Dall’Osto, M.: On the annual variability of
507 Antarctic aerosol size distributions at Halley Research Station, Atmospheric Chemistry
508 and Physics, 20, 4461–4476, <https://doi.org/10.5194/acp-20-4461-2020>, 2020.

509 Li, J., Wang, W., Li, K., Zhang, W., Peng, C., Zhou, L., Shi, B., Chen, Y., Liu, M.,
510 Li, H., and Ge, M.: Temperature effects on optical properties and chemical composition
511 of secondary organic aerosol derived from *n*-dodecane, Atmospheric Chemistry and
512 Physics, 20, 8123–8137, <https://doi.org/10.5194/acp-20-8123-2020>, 2020.

513 Li, J., Carlson, B. E., Yung, Y. L., Lv, D., Hansen, J., Penner, J. E., Liao, H.,
514 Ramaswamy, V., Kahn, R. A., Zhang, P., Dubovik, O., Ding, A., Lacis, A. A., Zhang,
515 L., and Dong, Y.: Scattering and absorbing aerosols in the climate system, Nat Rev
516 Earth Environ, 3, 363–379, <https://doi.org/10.1038/s43017-022-00296-7>, 2022.

517 Liu, Y., Zhou, Y., and Lu, J.: Exploring the relationship between air pollution and
518 meteorological conditions in China under environmental governance, Sci Rep, 10,
519 14518, <https://doi.org/10.1038/s41598-020-71338-7>, 2020.

520 Lou, M., Guo, J., Wang, L., Xu, H., Chen, D., Miao, Y., Lv, Y., Li, Y., Guo, X., Ma,
521 S., and Li, J.: On the Relationship Between Aerosol and Boundary Layer Height in
522 Summer in China Under Different Thermodynamic Conditions, Earth and Space
523 Science, 6, 887–901, <https://doi.org/10.1029/2019EA000620>, 2019.

524 Meng, H., Bai, G., and Wang, L.: Analysis of the spatial and temporal distribution
525 characteristics of AOD in typical industrial cities in northwest China and the influence
526 of meteorological factors, Atmospheric Pollution Research, 15, 101957,
527 <https://doi.org/10.1016/j.apr.2023.101957>, 2024.

528 Miao, Y. and Liu, S.: Linkages between aerosol pollution and planetary boundary
529 layer structure in China, Science of The Total Environment, 650, 288–296,
530 <https://doi.org/10.1016/j.scitotenv.2018.09.032>, 2019.

531 Murphy, D. M., Anderson, J. R., Quinn, P. K., McInnes, L. M., Brechtel, F. J.,
532 Kreidenweis, S. M., Middlebrook, A. M., Pósfai, M., Thomson, D. S., and Buseck, P.
533 R.: Influence of sea-salt on aerosol radiative properties in the Southern Ocean marine
534 boundary layer, Nature, 392, 62–65, <https://doi.org/10.1038/32138>, 1998.

535 Pei, Q., Saikawa, E., Kaspari, S., Widory, D., Zhao, C., Wu, G., Loewen, M., Wan,
536 X., Kang, S., Wang, X., Zhang, Y.-L., and Cong, Z.: Sulfur aerosols in the Arctic,
537 Antarctic, and Tibetan Plateau: Current knowledge and future perspectives, Earth-

- 538 Science Reviews, 220, 103753, <https://doi.org/10.1016/j.earscirev.2021.103753>, 2021.
- 539 Petäjä, T., Järvi, L., Kerminen, V.-M., Ding, A. J., Sun, J. N., Nie, W., Kujansuu,
540 J., Virkkula, A., Yang, X., Fu, C. B., Zilitinkevich, S., and Kulmala, M.: Enhanced air
541 pollution via aerosol-boundary layer feedback in China, *Sci Rep*, 6, 18998,
542 <https://doi.org/10.1038/srep18998>, 2016.
- 543 Radenz, M., Engelmann, R., Henning, S., Schmithüsen, H., Baars, H., Frey, M. M.,
544 Weller, R., Bühl, J., Jimenez, C., Roschke, J., Muser, L. O., Wullenweber, N.,
545 Zeppenfeld, S., Griesche, H., Wandinger, U., and Seifert, P.: Ground-based Remote
546 Sensing of Aerosol, Clouds, Dynamics, and Precipitation in Antarctica —First results
547 from the one-year COALA campaign at Neumayer Station III in 2023,
548 <https://doi.org/10.1175/BAMS-D-22-0285.1>, 2024.
- 549 Satheesh, S. K. and Krishna Moorthy, K.: Radiative effects of natural aerosols: A
550 review, *Atmospheric Environment*, 39, 2089–2110,
551 <https://doi.org/10.1016/j.atmosenv.2004.12.029>, 2005.
- 552 Schuster, G. L., Dubovik, O., and Holben, B. N.: Angstrom exponent and bimodal
553 aerosol size distributions, *Journal of Geophysical Research: Atmospheres*, 111,
554 <https://doi.org/10.1029/2005JD006328>, 2006.
- 555 Shaw, G. E.: Considerations on the origin and properties of the Antarctic aerosol,
556 *Reviews of Geophysics*, 17, 1983–1998, <https://doi.org/10.1029/RG017i008p01983>,
557 1979.
- 558 Simmons, J. B., Humphries, R. S., Wilson, S. R., Chambers, S. D., Williams, A.
559 G., Griffiths, A. D., McRobert, I. M., Ward, J. P., Keywood, M. D., and Gribben, S.:
560 Summer aerosol measurements over the East Antarctic seasonal ice zone, *Atmospheric
561 Chemistry and Physics*, 21, 9497–9513, <https://doi.org/10.5194/acp-21-9497-2021>,
562 2021.
- 563 Su, Y., Han, Y., Luo, H., Zhang, Y., Shao, S., and Xie, X.: Physical-Optical
564 Properties of Marine Aerosols over the South China Sea: Shipboard Measurements and
565 MERRA-2 Reanalysis, *Remote Sensing*, 14, 2453, <https://doi.org/10.3390/rs14102453>,
566 2022.
- 567 Sun, Y., Wang, Z., Fu, P., Jiang, Q., Yang, T., Li, J., and Ge, X.: The impact of
568 relative humidity on aerosol composition and evolution processes during wintertime in
569 Beijing, China, *Atmospheric Environment*, 77, 927–934,
570 <https://doi.org/10.1016/j.atmosenv.2013.06.019>, 2013.
- 571 Thakur, R.: Trace elemental variability in aerosols near the two Indian Antarctic
572 research stations during austral summer, No. 26, pp 61–74, 2019.

573 Thornhill, G., Collins, W., Olivié, D., Skeie, R. B., Archibald, A., Bauer, S., Checa-
574 Garcia, R., Fiedler, S., Folberth, G., Gjermundsen, A., Horowitz, L., Lamarque, J.-F.,
575 Michou, M., Mulcahy, J., Nabat, P., Naik, V., O'Connor, F. M., Paulot, F., Schulz, M.,
576 Scott, C. E., Séférian, R., Smith, C., Takemura, T., Tilmes, S., Tsigaridis, K., and Weber,
577 J.: Climate-driven chemistry and aerosol feedbacks in CMIP6 Earth system models,
578 *Atmos. Chem. Phys.*, 21, 1105–1126, <https://doi.org/10.5194/acp-21-1105-2021>, 2021.

579 Tian, B., Ding, M., Putero, D., Li, C., Zhang, D., Tang, J., Zheng, X., Bian, L., and
580 Xiao, C.: Multi-year variation of near-surface ozone at Zhongshan Station, Antarctica,
581 *Environ. Res. Lett.*, 17, 044003, <https://doi.org/10.1088/1748-9326/ac583c>, 2022.

582 Tomasi, C., Vitale, V., Lupi, A., Di Carmine, C., Campanelli, M., Herber, A.,
583 Treffeisen, R., Stone, R. S., Andrews, E., Sharma, S., Radionov, V., von Hoyningen-
584 Huene, W., Stebel, K., Hansen, G. H., Myhre, C. L., Wehrl, C., Aaltonen, V.,
585 Lihavainen, H., Virkkula, A., Hillamo, R., Ström, J., Toledano, C., Cachorro, V. E.,
586 Ortiz, P., de Frutos, A. M., Blindheim, S., Frioud, M., Gausa, M., Zielinski, T., Petelski,
587 T., and Yamanouchi, T.: Aerosols in polar regions: A historical overview based on
588 optical depth and in situ observations, *Journal of Geophysical Research: Atmospheres*,
589 112, <https://doi.org/10.1029/2007JD008432>, 2007.

590 Tomasi, C., Lupi, A., Mazzola, M., Stone, R. S., Dutton, E. G., Herber, A.,
591 Radionov, V. F., Holben, B. N., Sorokin, M. G., Sakerin, S. M., Terpigova, S. A.,
592 Sobolewski, P. S., Lanconelli, C., Petkov, B. H., Busetto, M., and Vitale, V.: An update
593 on polar aerosol optical properties using POLAR-AOD and other measurements
594 performed during the International Polar Year, *Atmospheric Environment*, 52, 29–47,
595 <https://doi.org/10.1016/j.atmosenv.2012.02.055>, 2012.

596 Udisti, R., Dayan, U., Becagli, S., Busetto, M., Frosini, D., Legrand, M., Lucarelli,
597 F., Preunkert, S., Severi, M., Traversi, R., and Vitale, V.: Sea spray aerosol in central
598 Antarctica. Present atmospheric behaviour and implications for paleoclimatic
599 reconstructions, *Atmospheric Environment*, 52, 109–120,
600 <https://doi.org/10.1016/j.atmosenv.2011.10.018>, 2012.

601 Virkkula, A., Grythe, H., Backman, J., Petäjä, T., Busetto, M., Lanconelli, C., Lupi,
602 A., Becagli, S., Traversi, R., Severi, M., Vitale, V., Sheridan, P., and Andrews, E.:
603 Aerosol optical properties calculated from size distributions, filter samples and
604 absorption photometer data at Dome C, Antarctica, and their relationships with seasonal
605 cycles of sources, *Atmospheric Chemistry and Physics*, 22, 5033–5069,
606 <https://doi.org/10.5194/acp-22-5033-2022>, 2022.

607 Walters, W. W., Michalski, G., Böhlke, J. K., Alexander, B., Savarino, J., and
608 Thiemens, M. H.: Assessing the Seasonal Dynamics of Nitrate and Sulfate Aerosols at
609 the South Pole Utilizing Stable Isotopes, *Journal of Geophysical Research:*
610 *Atmospheres*, 124, 8161–8177, <https://doi.org/10.1029/2019JD030517>, 2019.

611 Wang, X., Chen, L., Guo, K., and Liu, B.: Spatio-temporal trajectory evolution
612 and cause analysis of air pollution in Chengdu, China, *Journal of the Air & Waste*
613 *Management Association*, 72, 876–894,
614 <https://doi.org/10.1080/10962247.2022.2058642>, 2022.

615 Wang, Z., Bi, L., Yi, B., and Zhang, X.: How the Inhomogeneity of Wet Sea Salt
616 Aerosols Affects Direct Radiative Forcing, *Geophysical Research Letters*, 46, 1805–
617 1813, <https://doi.org/10.1029/2018GL081193>, 2019.

618 Weller, R. and Lampert, A.: Optical properties and sulfate scattering efficiency of
619 boundary layer aerosol at coastal Neumayer Station, Antarctica, *Journal of Geophysical*
620 *Research: Atmospheres*, 113, <https://doi.org/10.1029/2008JD009962>, 2008.

621 Weller, R., Wöltjen, J., Piel, C., Resenberg, R., Wagenbach, D., König-Langlo, G.,
622 and Kriews, M.: Seasonal variability of crustal and marine trace elements in the aerosol
623 at Neumayer station, Antarctica, *Tellus B*, 60, 742–752, <https://doi.org/10.1111/j.1600->
624 [0889.2008.00372.x](https://doi.org/10.1111/j.1600-0889.2008.00372.x), 2008.

625 Weller, R., Schmidt, K., Teinilä, K., and Hillamo, R.: Natural new particle
626 formation at the coastal Antarctic site Neumayer, *Atmospheric Chemistry and Physics*,
627 15, 11399–11410, <https://doi.org/10.5194/acp-15-11399-2015>, 2015.

628 Xu, G., Chen, L., Zhang, M., Zhang, Y., Wang, J., and Lin, Q.: Year-round records
629 of bulk aerosol composition over the Zhongshan Station, Coastal East Antarctica, *Air*
630 *Qual Atmos Hlth*, 12, 271–288, <https://doi.org/10.1007/s11869-018-0642-9>, 2019.

631 Xu, G., Chen, L., Xu, T., He, S., and Gao, Y.: Distributions of water-soluble ions
632 in size-aggregated aerosols over the Southern Ocean and coastal Antarctica, *Environ.*
633 *Sci.: Processes Impacts*, 23, 1316–1327, <https://doi.org/10.1039/D1EM00089F>, 2021.

634 Yan, J., Jung, J., Lin, Q., Zhang, M., Xu, S., and Zhao, S.: Effect of sea ice retreat
635 on marine aerosol emissions in the Southern Ocean, Antarctica, *Sci Total Environ*, 745,
636 140773, <https://doi.org/10.1016/j.scitotenv.2020.140773>, 2020.

637 Yang, Y., Zhao, C., Wang, Q., Cong, Z., Yang, X., and Fan, H.: Aerosol
638 characteristics at the three poles of the Earth as characterized by Cloud–Aerosol Lidar
639 and Infrared Pathfinder Satellite Observations, *Atmospheric Chemistry and Physics*, 21,
640 4849–4868, <https://doi.org/10.5194/acp-21-4849-2021>, 2021.

641 Yu, L., Zhong, S., and Sun, B.: The Climatology and Trend of Surface Wind Speed
642 over Antarctica and the Southern Ocean and the Implication to Wind Energy
643 Application, *Atmosphere*, 11, 108, <https://doi.org/10.3390/atmos11010108>, 2020.

644 Zhang, F.: Factors Influencing the Spatio–Temporal Variability of Aerosol Optical
645 Depth over the Arid Region of Northwest China, *Atmosphere*, 15, 54,

646 <https://doi.org/10.3390/atmos15010054>, 2024.

647 Zhang, M., Chen, L., Xu, G., Lin, Q., and Liang, M.: Linking Phytoplankton
648 Activity in Polynyas and Sulfur Aerosols over Zhongshan Station, East Antarctica,
649 Journal of the Atmospheric Sciences, 72, 4629–4642, [https://doi.org/10.1175/JAS-D-](https://doi.org/10.1175/JAS-D-15-0094.1)
650 15-0094.1, 2015.

651